



RESEARCH ARTICLE

# Influences of buildings on urban heat island based on 3D landscape metrics: an investigation of China's 30 megacities at micro grid-cell scale and macro city scale

Xiaoyu Yu · Yue Liu · Zhonghao Zhang · Rui Xiao

Received: 19 January 2021 / Accepted: 1 June 2021 / Published online: 12 June 2021  
© The Author(s), under exclusive licence to Springer Nature B.V. 2021

## Abstract

**Context** The building landscape greatly affects the urban heat island (UHI), especially in three-dimensional (3D) space, by changing the energy flow between the land surface, the building surface and the lower atmosphere.

**Objectives** This study quantitatively analyzed the relationship between the 3D spatial pattern of buildings and UHI in China's 30 provincial capitals/municipalities and discussed them at grid-cell scale and city scale, respectively.

**Methods** In consideration of the spatial heterogeneity of the urban environment, Geographically

Weighted Regression Model (GWR) was selected to identify the effects of 3D building landscape pattern on summer UHI among 30 megacities of China at both micro grid-cell scale and macro city scale. Nine landscape metrics that used to describe the 3D structure of buildings and the UHI that calculated by hot-spot analysis were collected as input variables.

**Results** The floor area ratio (FAR), the average height (AH), and the space congestion degree (SCD) are the most influential factors affecting UHI. AH and SCD are negatively correlated with UHI, while FAR is the opposite. However, these relationships are not static, and they will change when interfered with other factors. The relationship between FAR and UHI becomes negative in the case of relatively low FAR value. In areas with low building coverage ratio, AH is positively correlated with UHI.

**Conclusions** The results of this study revealed the complicated association between the 3D building spatial pattern and UHI at micro and macro urban contexts, which was significant for decision-makers to formulate policies based on local conditions.

X. Yu · Y. Liu · R. Xiao (✉)  
School of Remote Sensing and Information Engineering,  
Wuhan University, No. 129 Luoyu Rd, Wuhan 430079,  
China  
e-mail: rxiao@whu.edu.cn

X. Yu  
e-mail: yuxiaoyu@whu.edu.cn  
Y. Liu  
e-mail: yliu\_rs@whu.edu.cn

Z. Zhang  
Institute of Urban Studies, School of Environmental and  
Geographical Sciences, Shanghai Normal University,  
Shanghai 200234, China  
e-mail: zzh87@shnu.edu.cn

Z. Zhang · R. Xiao  
School of Life Sciences and School of Sustainability,  
Arizona State University, Tempe, AZ 85287, USA

**Keywords** Urban heat island · 3D building landscape metrics · Geographically Weighted Regression Model · Micro grid-cell scale · Macro city scale

## Introduction

Urban heat island (UHI) is a phenomenon where the temperature in urban areas is higher than that in surrounding suburban/rural areas (Oke 1973). It has been recognized that the increase in buildings, the population explosion, and the land use transformation, caused by rapid urbanization, have important impacts on UHI (Sun et al. 2019; Cao et al. 2020). The United Nations reported that the world population will increase from 7.7 billion to 9.7 billion in the next 30 years (United Nations 2019), which will undoubtedly strengthen the UHI. UHI causes a series of ecological and environmental problems, such as water and air pollution (Huang and Cadenasso 2016; Yang et al. 2019), climate changes and biodiversity reduction (Jun-Hyun et al. 2016). These problems will further lead to increased energy consumption (Zhou et al. 2014a; Ma et al. 2016), heat stress and mortality (Li et al. 2011), with profound impacts on residents' life comfort and regional sustainability (Wu 2010, 2014). Improving urban sustainability has become one of the United Nations sustainable development goals (Kong et al. 2020). Therefore, a better understanding of the UHI and its influencing factors can support future climate mitigation actions and human adaptive strategies to achieve urban sustainability (Zhou et al. 2014b; Ma et al. 2016).

Generally, the factors affecting the UHI can be divided into two main groups. The first group includes biophysical factors that are not associated with human existence or activities, such as climatic zone, season, time of the day and wind conditions (Wang et al. 2016). The second group includes factors related to the urban landscape, such as impervious surface, vegetation cover, and water bodies (Connors et al. 2013; Alavipanah et al. 2018). Among these factors, it is recognized that impervious surface taking over natural land do contribute a lot to UHI effect (Huang and Cadenasso 2016; Chapman et al. 2017). Buildings are a key component of the impervious surface and therefore an important contributor to the UHI (Li et al. 2011; Huang and Wang 2019; Sun et al. 2020). As for the analysis of the relationships between buildings and the UHI, previous studies mainly focused on the effects of two-dimensional (2D) landscape metrics of buildings on the UHI, such as patch density (PD), edge density (ED), landscape shape index (LSI), largest patch index (LPI) and

contagion index (CONTAG) (Li et al. 2011; Huang and Wang 2019; Jia and Wang 2020). In recent years, analyzing the relationships between the three-dimensional (3D) landscape metrics of the buildings and the UHI has become a research hotspot. Hu et al. (2020) indicates that the height and shape of the buildings in Beijing will affect the surface albedo, which in turn affects UHI. Sky view factor (SVF) can be used to determine the absorption of solar radiation on urban surfaces and the total turbulent heat transport, which directly affects the UHI in Columbus and Wuhan, respectively (Chun and Guldmann 2014; Yin et al. 2018). Tian et al. (2019) shows that urban geometry, which is related to the height and spacing of buildings (sky openness), influences air circulation and wind flow, and therefore the UHI in Beijing. All these studies have brought useful references for the development of the UHI research, but there are still a few shortcomings. First, previous studies usually focus on the impact of the coupling of 2D and 3D landscape metrics on the UHI (Berger et al. 2017; Hu et al. 2020; Yu et al. 2020). Few attempts have been made to select a comprehensive set of 3D landscape metrics to conduct a thorough and exclusive analysis of the impact of 3D spatial pattern of buildings on UHI. Second, an investigation to analyze the effects of 3D spatial pattern of buildings on the UHI at large scale is still missing. A majority of the case studies have been only conducted in a single city, so the conclusions lack universality and it is difficult to summarize general rules for improving the thermal environment in different cities (Yin et al. 2018; Huang and Wang 2019; Yu et al. 2020).

Current methods for quantitatively exploring the relationship between UHI and its influencing factors are mainly correlation analysis and regression analysis. For example, Morabito et al. (2016) used the OLS model to explore the impact of built-up surfaces on LST in Italy, and Zhou et al. (2014a) introduced Pearson's correlation coefficients and stepwise multiple linear regressions to investigate the various drivers on UHI in China 32 cities. Yin et al. (2018) employed spatial error model to analyze the relationship between urban form and UHI in Wuhan. Although these global regression models were well established, the spatial non-stationarity in the relationships between variables was ignored. By establishing local regression models for different regions within a specific spatial range (Fotheringham et al. 2004), the geographically

weighted regression (GWR) model fully considers the local effects and the spatial heterogeneity of the relationships between UHI and its factors which can accurately and effectively reflect those relationships. The GWR model has been proven to perfectly evaluate the impact of driving factors on UHI in a single city (Li et al. 2010; Zhang et al. 2019b; Jia and Wang 2020), urban agglomeration (Wang et al. 2016), and even the global cities (Li et al. 2020a). Although these studies have made great contributions to reveal the relationships between UHI and its influencing factors, they only explored these relationships at a single scale, and few studies could take into account analyzing these relationships at both micro and macro scales. Simultaneously analyzing the relationships between UHI and the 3D structure of buildings at both macro and micro scales can provide macro control measures and micro layout suggestions for landscape planners, which can better alleviate the UHI.

Therefore, to solve these issues exist in previous studies, this study selected 30 capitals/municipalities in China as study area to reveal the relationships between 3D landscape metrics and the UHI at both macro and micro scales, in order to provide reliable support for urban landscape planning to improve the thermal environment, and thus achieve sustainable urban development. Specifically, this study aimed to: (1) analyze 3D spatial pattern of buildings in China's 30 capitals/municipalities, (2) investigate the intensity and spatial distribution of UHI, and (3) provide an innovative way to use the GWR model to explore the relationships between 3D building landscape metrics and UHI at both micro grid-cell scale and macro city scale.

## Study area and data

### Study area

Our study area covered China's 30 major cities (Fig. 1), including 4 directly-controlled municipalities and 26 provincial capitals (Urumqi was not considered due to the data scarcity). The terrain of China is high in west but low in east, so the western cities are dominated by plateaus and hills, while the eastern cities are mostly plains and basins. Meanwhile, these cities located in different climate regions, ranging from the tropical to alpine, from hot to cold

and from humid to drought (Zhou et al. 2014a). The eastern, central-southern and southwestern cities of China have a typical hot and humid climate, while northeastern, northern and northwestern cities have typical humid and cold, semi-humid/semi-temperate and arid climates, respectively (Zhou et al. 2014a). In this way, there exist significant differences in urban spatial patterns between cities (Yue et al. 2019).

The provincial capitals are usually highly urbanized, with large populations and developed economies (Fang et al. 2015). As the main commercial centers of their respective provinces, the cities play a leading role in the economic development of the province and even the country, and also drive the economic development of the surrounding underdeveloped areas. However, in recent years, the rapid increases in urban population and frequent human activities have led to the accumulation of a large amount of heat energy in urban areas, which exacerbated the UHI. Therefore, it is necessary to explore the UHI intensity and its influence factors in core urban areas of these 30 cities.

### Datasets

The 3D building data in 2018 were derived from the online map service platform Gaode maps (<http://lbs.amap.com/>) through the open API by Python programming, which contains the outline and total number of floors information of the buildings in the urban area. The number of floors is multiplied by 3 m to get the building height information (Sun et al. 2020). The required land surface temperature (LST) data were obtained from Landsat 8 thermal infrared sensor (TIRS) images of a spatial resolution of 100 m and 16-day interval. The data were collected from the U.S. geological survey (USGS) website ([www.earthexplorer.usgs.gov](http://www.earthexplorer.usgs.gov)) in summer (from June to September) from 2016 to 2018, because the most intense UHI occurs in summer (Yang et al. 2019). The data has been officially resampled to 30 m using a cubic convolution algorithm by the USGS. After radiation correction and geometric correction, based on the Landsat Data Users Handbook Version 5.0 (NASA 2019), the LST was retrieved as follows:

$$LST = \frac{T_B}{1 + (\lambda \times T_B / \rho) \ln \epsilon} \quad (1)$$

where  $T_B$  is the brightness temperature; and  $\lambda$  is the wavelength of the radiation emission

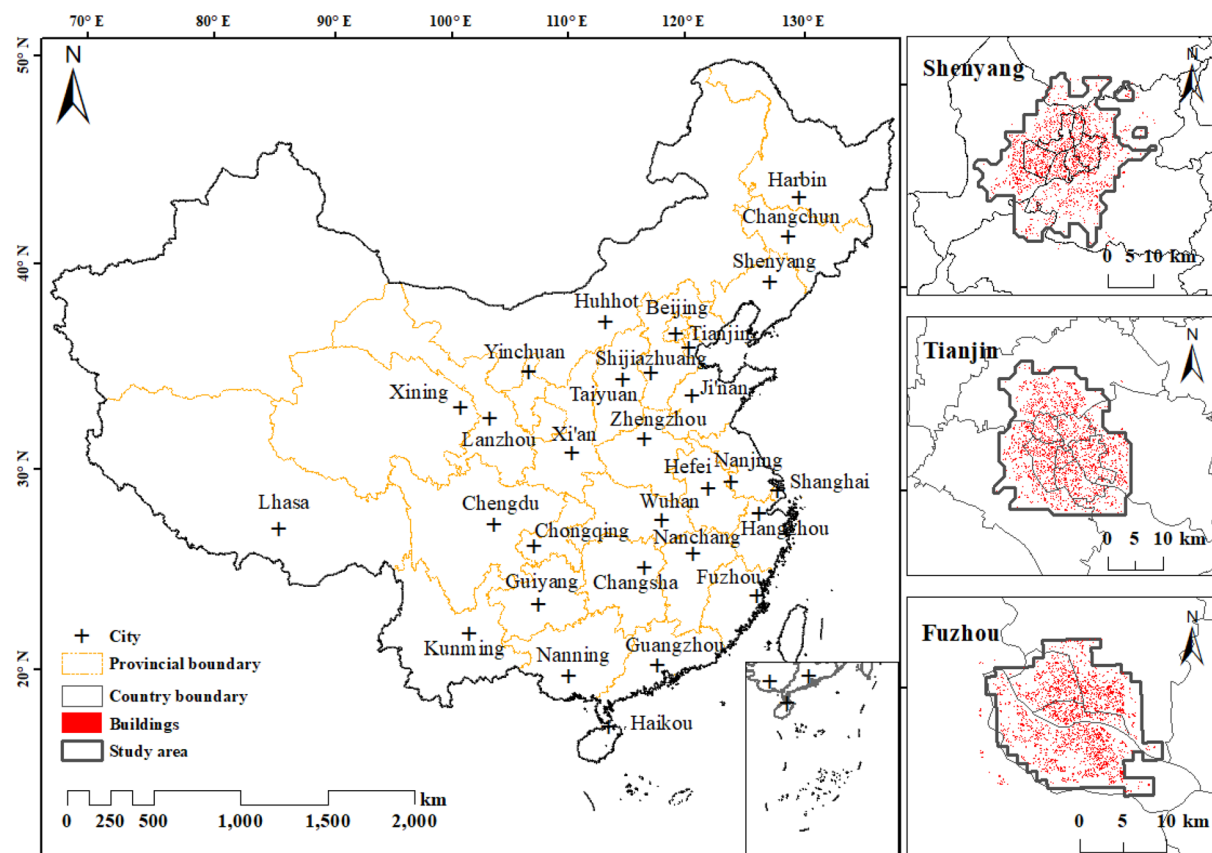


**Fig. 1** Locations of the 30 major cities and examples of the delineation of study area in Shenyang, Tianjin, and Fuzhou

( $10.8 \mu\text{m}$ ).  $\rho = (h \times c)/\delta = 1.438 \times 10^{-2} \text{ mK}$ , where  $h$  is Planck's constant ( $6.626 \times 10^{-34} \text{ Js}$ ),  $c$  is the speed of light ( $2.998 \times 10^8 \text{ ms}^{-1}$ ), and  $\delta$  is the Boltzmann constant ( $1.381 \times 10^{-23} \text{ JK}^{-1}$ ) (Peng et al. 2018).  $\epsilon$  is the surface emissivity, which were determined by the normalized difference vegetation index (NDVI) (Defries and Townshend 2007). To make the LST data more precise and convincing, the LSTs acquired in 3-year summer were averaged.

## Methods

### Urban area extraction and grid partition

The urban area for each city was extracted by referring to Zhou et al. (2014a). First, using a  $1 \text{ km} \times 1 \text{ km}$  moving window method, a built-up intensity (BI) map was generated with impervious surface data. Then, areas with BI value  $> 50\%$  were selected as high-

intensity built-up land, and these high-intensity built-up land areas were aggregated to form a compact urban area. Finally, the boundary of the urban area is constrained by the scope of the 3D building data. Due to the limitation of data sources, areas with no building data or incomplete building data (such as urban fringe zone) will be excluded from the scope of the city's urban area. The final urban areas for three representative cities of China (Shenyang, Tianjin, and Fuzhou) are shown in Fig. 1.

In landscape ecology, scale refers to the grain and extent in the spatial and temporal dimensions (Wu 2004), which refers to the size of the grid in our study. For comprehensive consideration, we chose a grid size of  $1 \text{ km} \times 1 \text{ km}$ . (1) On the one hand, the smaller the input grid size is, the less noise and more details of 3D landscape metrics are retained (Weng 2007). On the other hand, our study area involves the core urban areas of 30 cities, and the largest central urban area appears in Shanghai, reaching  $1119 \text{ km}^2$ . If the grid

size is too small, a huge amount of data will be generated, causing a data load, so 1 km is a compromise choice. (2) Previous studies have proved that 1 km is a suitable research scale for exploring the relationship between the 3D landscape metrics and UHI (Wu et al. 2013; Wu and Lung 2016). (3) The selected grid-cell scale must not only ensure a sufficient sample size for further regression analysis, but also that it cannot exceed the processing memory of the GWR4.0 software.

### Selection of 3D landscape metrics

Based on the principles of generality, representativeness, and commonality, our study proposes a comprehensive set of 3D landscape metrics to analyze the 3D building environment of the city (Table 1). From previous literature, the following nine 3D landscape metrics are considered: average height (AH, m),

height coefficient of variation (CH), high building ratio (HBR), average volume (AV, m<sup>3</sup>), space congestion degree(SCD), average building shape coefficient (BSC), building evenness index (BEI), floor area ratio (FAR), Cubic index (CI) (Zhang and Hu 2013; Berger et al. 2017; Liu et al. 2017, 2020a; Huang and Wang 2019; Hu et al. 2020). These metrics describe the different characteristics of the building, such as height, volume, shape, density, etc., and they have been proved to be related to UHI (Berger et al. 2017; Alavipanah et al. 2018). The formulas and description of each landscape metric are shown in Table 1.

### Calculation of UHI

Considering the inability to accurately distinguish the boundaries between the urban and suburban areas of 30 cities, the traditional definition of UHI (temperature difference between urban and suburban areas) is not

**Table 1** 3D landscape metrics selected in this study

Metrics	Abbreviation	Formula	Description	References
Average height	AH	$AH = \frac{1}{n} \sum_{i=1}^n H_i$	The average height of total buildings	Berger et al. (2017), Hu et al. (2020)
Height coefficient of variation	CH	$CH = \frac{1}{AH} \left[ \frac{1}{n} \sum_{i=1}^n (H_i - AH)^2 \right]^{\frac{1}{2}}$	The differences in the height of urban buildings	Liu et al. (2017), Huang and Wang (2019)
High building ratio	HBR	$HBR = N_i/N$	Proportion of buildings over 24 m	Liu et al. (2017)
Average volume	AV	$AV = \frac{1}{n} \sum_{i=1}^n V_i$	The average volume of total buildings	Berger et al. (2017)
Space congestion degree	SCD	$SCD = \sum_{i=1}^n (F_i \times H_i) / (\sum_{i=1}^n F_i \times H_{max})$	The congestion degree of the building in three-dimension space	Zhang and Hu (2013)
Average building shape coefficient	BSC	$BSC = \frac{1}{n} \sum_{i=1}^n \frac{S_i}{V_i}$	Reflect the size of the spatial heat dissipation area and the energy consumption of the buildings	Huang and Wang (2019)
Building evenness index	BEI	$BEI = \sqrt{\left[ \sum_{i=1}^n (V_i - AV) \right]^2 / A}$	The evenness of the building in three-dimension space	Zhang and Hu (2013)
Floor area ratio	FAR	$FAR = \sum_{i=1}^n (H_i / C \times F_i) / A$	Building area of unit land area	Liu et al. (2017, 2020a)
Cubic index	CI	$CI = \frac{\sum_{i=1}^n V_i}{H_{max} \times A} \times 100\%$	The proportion of buildings in the total building space	Berger et al. (2017)

Hi, Vi, Fi, and Si are the height, volume, floor area, and surface area of the i-th building, n is the number of buildings, A is the area of the analysis area, C = 3.0 m is a constant, and Hmax is the maximum height of the total buildings

suitable for this research, so the hot spot analysis is used to explore the thermal environment inside the city. The Getis-Ord Gi\* statistics (Getis and Ord 1992; Ord and Getis 1995) are used for hot spot analysis, which can identify spatial clusters of statistically significant areas with high or low attribute values. The Getis-Ord Gi\* statistics are actually a Gi\*Z score. The z-score would have to be less than  $-2.58$  or greater than  $2.58$  to be statistically significant, which correspond to the 99% confidence level. In this study, areas with a Z score  $> 2.58$  are defined as significant aggregation of high temperature (hotspot), while the areas with a Z score less than  $-2.58$  are defined as significant aggregation of low temperature (coldspot). The Hot Spot Analysis tool (Getis-Ord Gi\*) within ArcGIS version 10.2 software are used for the Gi\*Z score calculation, and the spatial weight was based on Queen's adjacency connectivity matrix. The formula of Gi\*Z score is as follows:

$$G_i*Z_{score} = \frac{\sum_{j=1}^n w_{i,j}x_j - \bar{X} \sum_{j=1}^n w_{i,j}}{S \sqrt{\frac{n \sum_{j=1}^n w_{i,j}^2 - \left(\sum_{j=1}^n w_{i,j}\right)^2}{n-1}}} \quad (2)$$

$$\bar{X} = \frac{\sum_{j=1}^n x_j}{n} \quad (3)$$

$$S = \sqrt{\frac{\sum_{j=1}^n x_j^2}{n} - \bar{X}^2} \quad (4)$$

where  $w_{i,j}$  is the spatial weight derived from Queen's adjacency connectivity matrix between reference point i and n points within defined distance from point i,  $x_j$  is temperature value at point j and  $X$  is mean temperature.

In this study, we defined magnitude of intra-urban thermal differences as UHI for a city, which is the difference of the mean temperature between hotspot and coldspot areas (Feyisa et al. 2016). The UHI is given by:

$$UHI = Tmean_{Gi*Zscore > 2.58} - Tmean_{Gi*Zscore < -2.58} \quad (5)$$

where UHI is the heat island intensity for a city,  $Tmean_{Gi*Zscore > 2.58}$  is the mean surface temperature of areas with  $Gi*Zscore > 2.58$ , and  $Tmean_{Gi*Zscore < -2.58}$  is the mean surface temperature of areas with  $Gi*Zscore$  less than  $-2.58$ .

For the subsequent GWR analysis, the UHI of each grid (G\_UHI) also needs to be calculated as the dependent variable. The G\_UHI is calculated as follows:

$$G_UHI_i = T_i - Tmean_{Gi*Zscore < -2.58} \quad (6)$$

where  $G_UHI_i$  is the urban heat island intensity for the i-th grid,  $T_i$  is the mean temperature of the i-th grid, and  $Tmean_{Gi*Zscore < -2.58}$  is the mean surface temperature of areas with  $Gi*Zscore$  less than  $-2.58$ .

### Geographically weighted regression (GWR)

As a local regression model, GWR is an extension of the global regression model. The premise of establishing a global model is that the variables are spatially homogeneous among various regions. However, this condition is usually difficult to meet, because many processes observed in nature are spatially heterogeneous, especially for UHI (Szymanowski and Kryza 2012). GWR is a local modeling tool optimized based on the global regression model, which complements the global model by providing a set of coefficients for each geographical unit to reveal the spatial variability of the observations (Brunsdon et al. 1996). The GWR model can be expressed as follows:

$$y_i = \beta_0(u_i, v_i) + \sum_{k=1}^n \beta_k(u_i, v_i)x_{ik} + \epsilon_i \quad (7)$$

where  $y_i$  is the dependent variable of the i-th geographical unit,  $\beta_0$  and  $\beta_k$  are the estimated coefficients,  $(u_i, v_i)$  is the coordinates of the i-th geographical unit,  $x_{ik}$  is the k-th explanatory variables at i-th geographical unit,  $\epsilon_i$  is the random error term at the i-th geographical unit. In order to estimate the parameters  $\beta_0$  and  $\beta_k$  in the equation, the spatial weight of the explanatory variables needs to be calculated. The observation point is usually weighted according to the proximity to a specific point i, that is, the distance between the observation point and the point i determines the weight given to the observation point; the larger weight usually corresponds to closer distances. Therefore, the spatial weight of explanatory variables is not constant, but a distance attenuation function of the position. In this study, decreasing kernel function of Gaussian was used to calculate the weights (Fotheringham et al. 2004), and the formula is as follows:

$$w_{ij} = \exp\left(-\frac{1}{2}\left(\frac{d_{ij}}{b}\right)^2\right) \quad (8)$$

where  $w_{ij}$  is the geographical weight of the j-th geographical unit with regard to geographical unit i,  $d_{ij}$  is the Euclidean distance between geographical units i and j, b is the bandwidth, and the optimal bandwidth in our research is based on the golden section search under the Akaike Information Criterion (AIC) (Akaike 1998).

## Results

### Statistics of 3D landscape metrics

Figure 2 shows the spatial distribution of the average 3D landscape metrics in each city, and the statistics of all the cities. The 3D landscape metrics shows obvious spatial heterogeneity across 30 cities. AH (Fig. 2a), HBR (Fig. 2c), AV (Fig. 2d), and SCD (Fig. 2e) shows similar spatial patterns. Cities in the southwest (Chongqing, Kunming, and Guiyang) have higher AH, HBR, AV and SCD values, while lower values appear in the north China cities. This is because that the cities in southwest China are mountainous and less plain, which limits the horizontal expansion of the city, so the buildings extend in height, resulting in higher AH, HBR, AV and SCD. In contrast, the value of CH (Fig. 2b), and BSC (Fig. 2f) is higher in the north

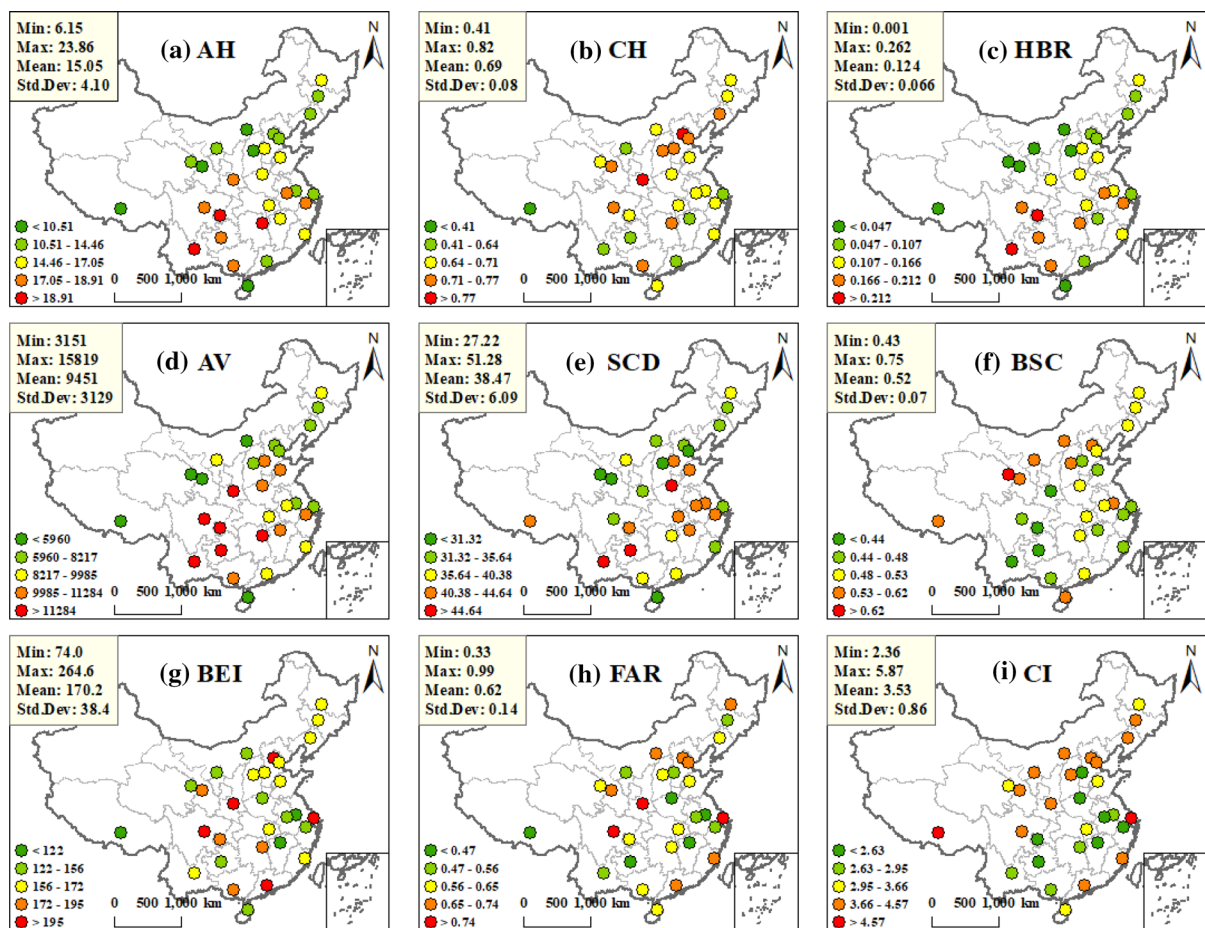


**Fig. 2** The spatial distribution of the mean for nine 3D landscape metrics in 30 cities

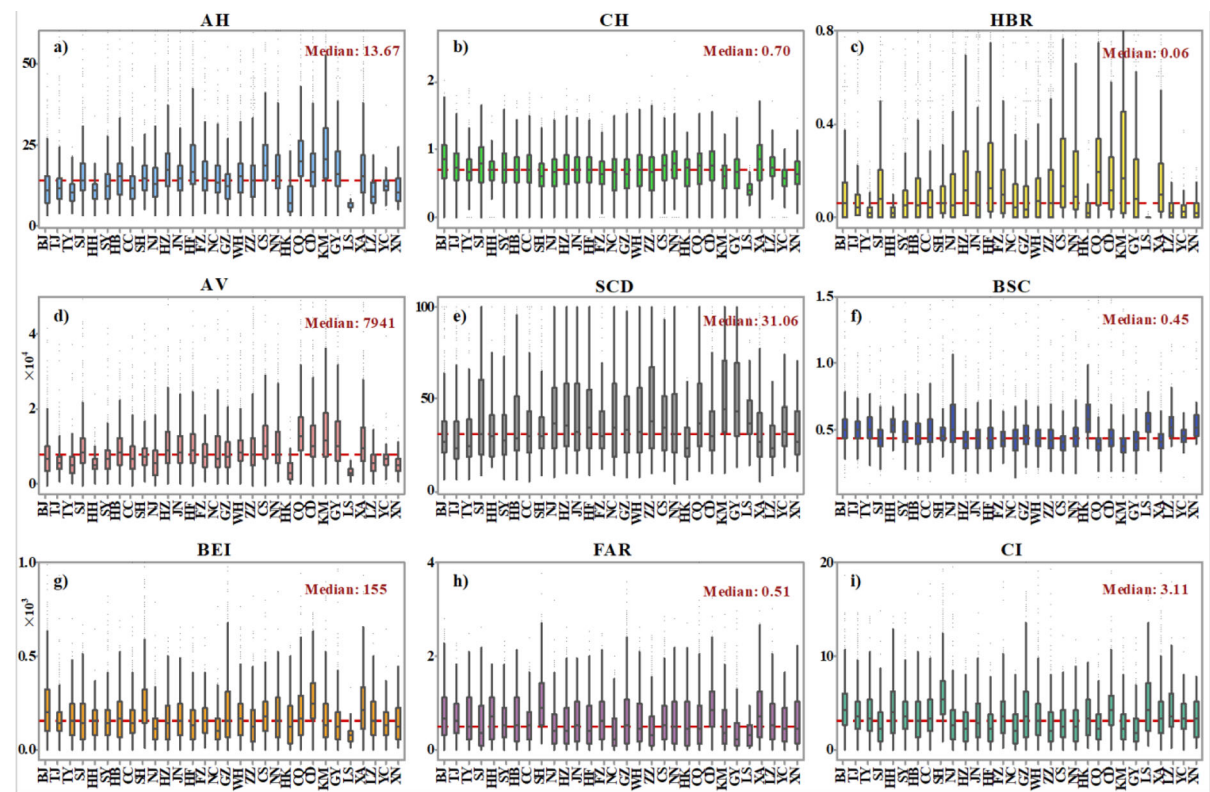
cities, and lower in the south cities, indicating that the buildings in northern cities vary greatly in height and have more complex shapes. For BEI, high value means uneven distribution of buildings. The BEI (Fig. 2g) for three super large cities Beijing (223.4), Shanghai (250.4) and Guangzhou (216.4) are extremely exceeding the average of all cities (170.2), which is due to the lots of large buildings and their concentrated distribution in space. The spatial distribution of FAR (Fig. 2h) is consistent with that of CI (Fig. 2i), with higher values in northern China cities and lower values in southern China cities, except Shanghai, Fuzhou, Guangzhou and Chengdu.

Figure 3 displays the statistical description of 3D landscape metrics of all grids within each city. For AH (Fig. 3a), HBR (Fig. 3c), AV (Fig. 3d), SCD (Fig. 3e), BEI (Fig. 3g) and CI (Fig. 3i), the statistics of the 3D landscape metrics at the grid-cell scale is consistent with that at the city scale, that is, cities with higher mean 3D landscape metrics at the city scale

generally have higher values in their most internal grids. However, in a city with higher mean 3D landscape metrics at the city scale, the difference in landscape metrics between the internal grids is greater than that of other cities. But for CH (Fig. 3b), BSC (Fig. 3f), and FAR (Fig. 3h), with the exception of several cities, the difference of the internal grids' 3D landscape metrics between cities is minuscule, which does not show the law of obvious regional differences at the city scale.

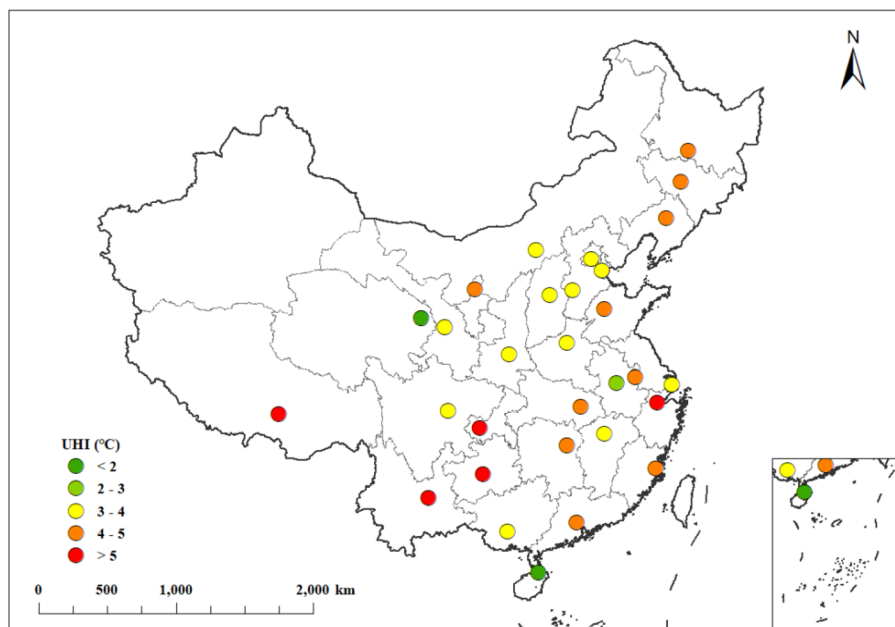
#### Spatial distribution of UHI

Figure 4 shows that the summer UHI is intense in China's 30 cities and spatially varies significantly, ranging from 1.99 °C (Haikou) to 8.08 °C (Kunming). The UHI differs greatly by geographical location and the UHI for cities located in the same geographical location is similar. The UHI of three cities (Shenyang: 4.62 °C, Changchun: 4.86 °C, and Harbin: 4.40 °C) in



**Fig. 3** Statistics of 3D landscape metrics in 30 city grids (*BJ* Beijing, *TJ* Tianjin, *TY* Taiyuan, *SJ* Shijiazhuang, *HH* Huhhot, *SY* Shenyang, *HB* Harbin, *CC* Changchun, *SH* Shanghai, *NJ* Nanjing, *HZ* Hangzhou, *JN* Jinan, *HF*/*FZ* Fuzhou, *NC*

Nanchang, *GZ* Guangzhou, *WH* Wuhan, *ZZ* Zhengzhou, *CS* Changsha, *NN* Nanning, *HK* Haikou, *CQ* Chongqing, *CD* Chengdu, *KM* Kunming, *GY* Guiyang, *LS* Lhasa, *XA* Xi'an, *LZ* Lanzhou, *YC* Yinchuan, *XN* Xining)



**Fig. 4** Spatial distribution of UHI in 30 cities

the northeast China is all between 4 and 5 °C, and five cities (Beijing: 3.69 °C, Tianjin: 3.51 °C, Shijiazhuang: 3.52 °C, Xi'an: 3.83 °C, and Huhhot: 3.88 °C) located in north China also have similar UHI. Overall, the cities located in the southern and northeastern parts suffer from more intense UHI than those in the northern and northwestern cities in China.

Figure 5 displays the spatial distribution of hotspot analysis results for 30 cities, which can be used to explore the spatial heterogeneity of UHI. Among 30 cities, hotspot analysis results of 23 cities shows that the hotspots are mainly concentrated near the city center, while the cold spots are scattered around the edge of the city. In the remaining 7 cities (Chengdu, Chongqing, Fuzhou, Guangzhou, Hangzhou, Lanzhou, and Wuhan), the hotspots are no longer concentrated in the city center. Instead, they are scattered in the study area. This may be because that they are typical polycentric cities, so hotspots are scattered across multiple sub-central regions.

#### GWR results and analysis

All the variance inflation factor values (VIF) calculated by the least square regression range from 1.018 to 6.371, which are all  $< 7$ , indicating that the independent variables did not suffer from the problem

of severe multi-collinearity, so all 3D landscape metrics can be input into the GWR model to explore its impact on UHI.

Figure 6a displays the adjusted  $R^2$  of 30 cities. It can be found that the GWR model performs well in exploring the relationship between the 3D landscape metrics and UHI, with adjusted  $R^2$  ranging from 0.307 (Wuhan) to 0.747 (Changchun). Among them, the adjusted  $R^2$  of 73.3% cities is  $> 0.5$ , and 83.3% cities adjusted  $R^2$  is  $> 0.4$ . From Fig. 6a, it is noted that higher adjusted  $R^2$  values mainly appear in northern and northeastern China cities, indicating the stronger explanatory power and impact of selected 3D landscape metrics on UHI, while the lower adjusted  $R^2$  values demonstrate a worse regression fit in Lanzhou (0.314), Yinchuan (0.393), Wuhan (0.307), Nanchang (0.387), and Hangzhou (0.356). The statistics of the local  $R^2$  values within each city at grid-cell scale is shown in Fig. 6b, which is slightly different from that at city scale. The grid-cell scale statistics show that the worst fitting degree for GWR model occurs in Hangzhou and Wuhan, where more than 60% of the regions have local  $R^2$  values below 0.4. The 3D landscape metrics of Taiyuan (95.59%), Lhasa (91.89%), Changchun (89.15%), and Fuzhou (88.32%) have a significant correlation with the

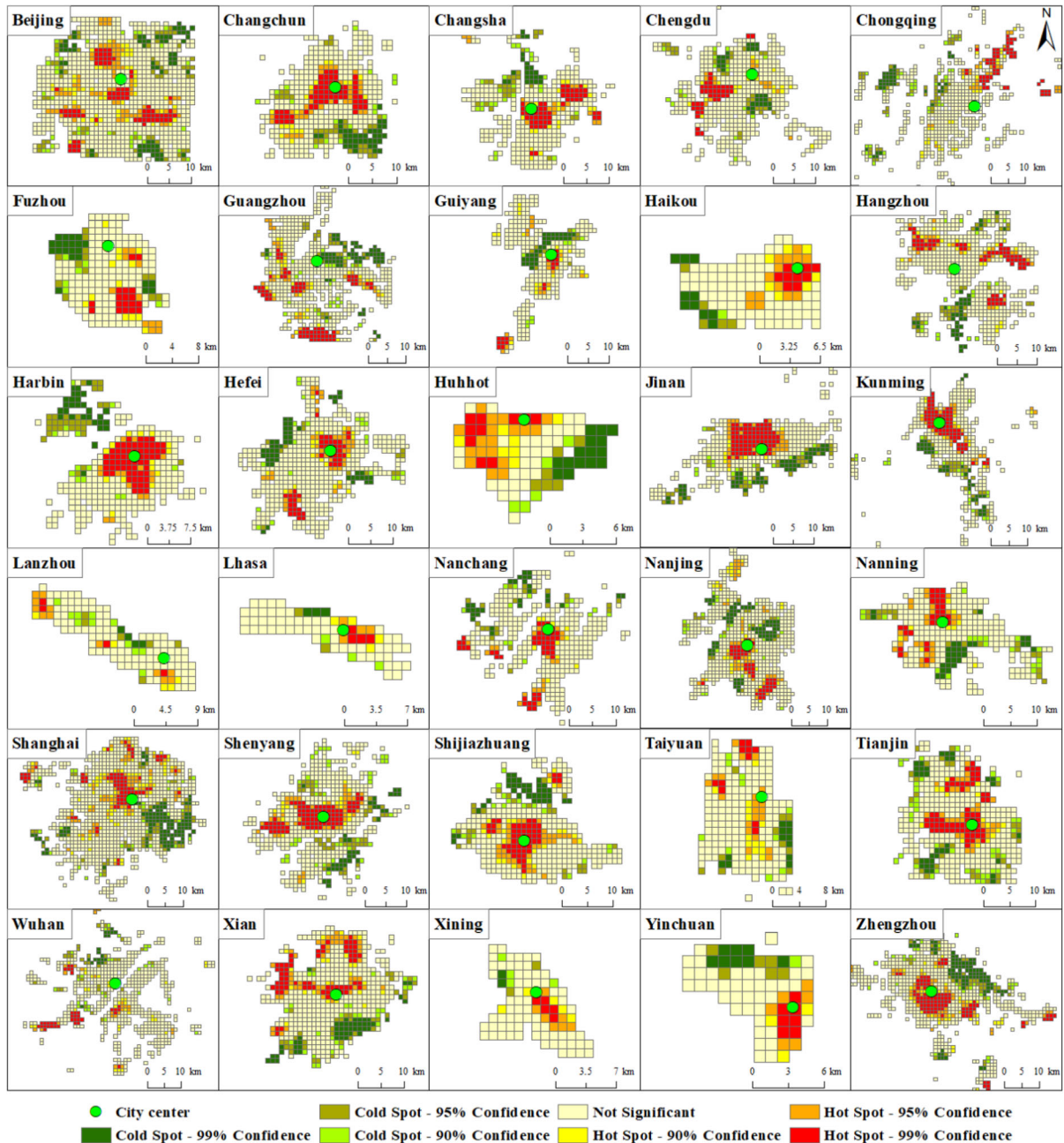


**Fig. 5** Spatial distribution of hotspot analysis results in the internal grids of 30 cities

UHI, with local  $R^2$  of more than 80% of areas exceeding 0.6.

Before the GWR analysis, the independent variables have been standardized, so the absolute value of the regression coefficients can measure the importance of its impact on UHI. The variable with the largest absolute value of the coefficient is considered to be the

winning variable, which means it is the main factor affecting UHI at that position (Liu et al. 2020b). For a city, the variable with the largest proportion is regarded as the dominant variable in that city. As shown in Fig. 7a, FAR becomes the dominant variable in 10 cities, followed by AH, becoming the winning variable in 9 cities. Figure 7a also displays the spatial

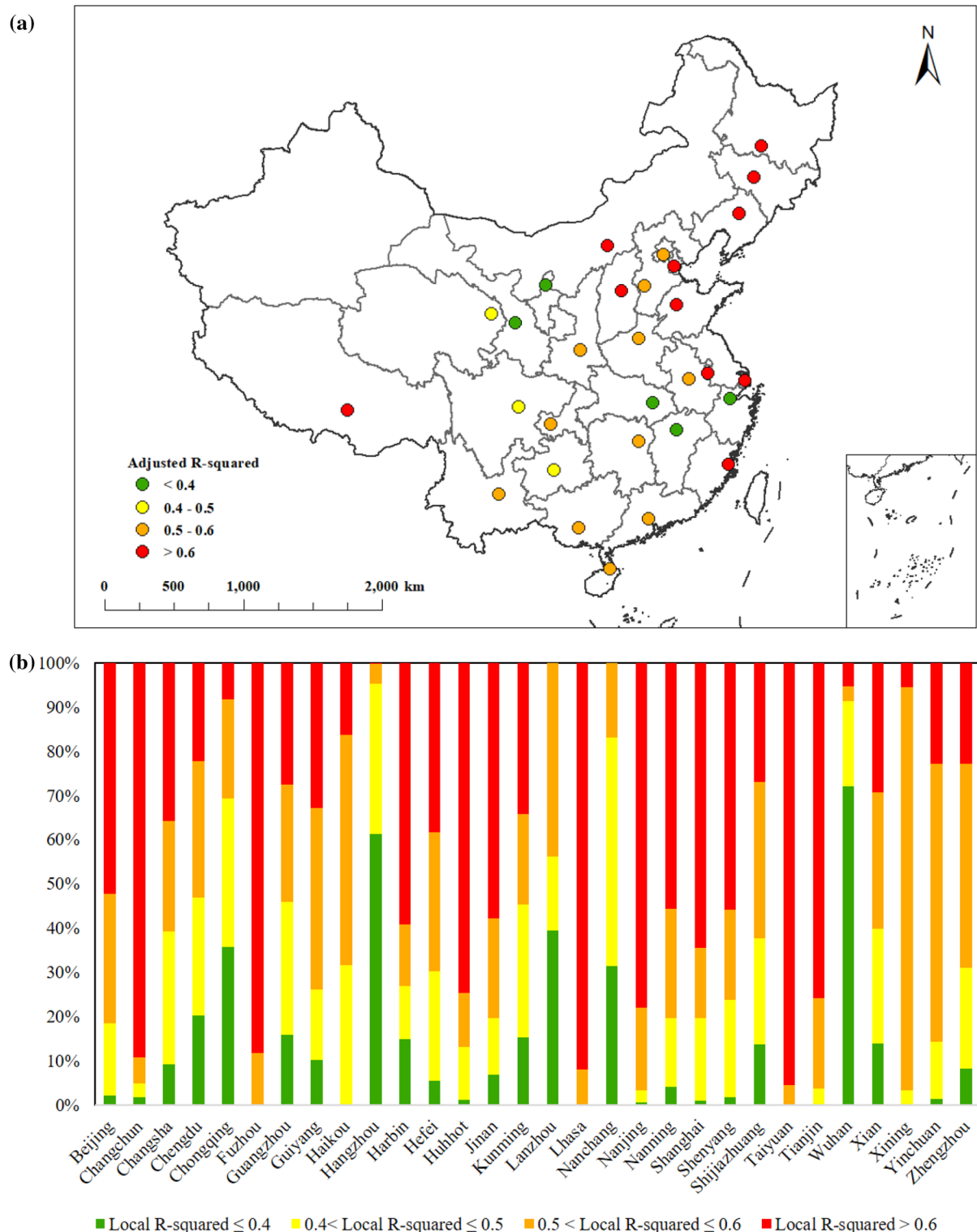


**Fig. 6** Statistics of the explanatory power of selected 3D landscape metrics on UHI. **a** Spatial distribution of adjusted  $R^2$  for 30 cities, **b** statistics of local  $R^2$  within each city at grid-cell scale

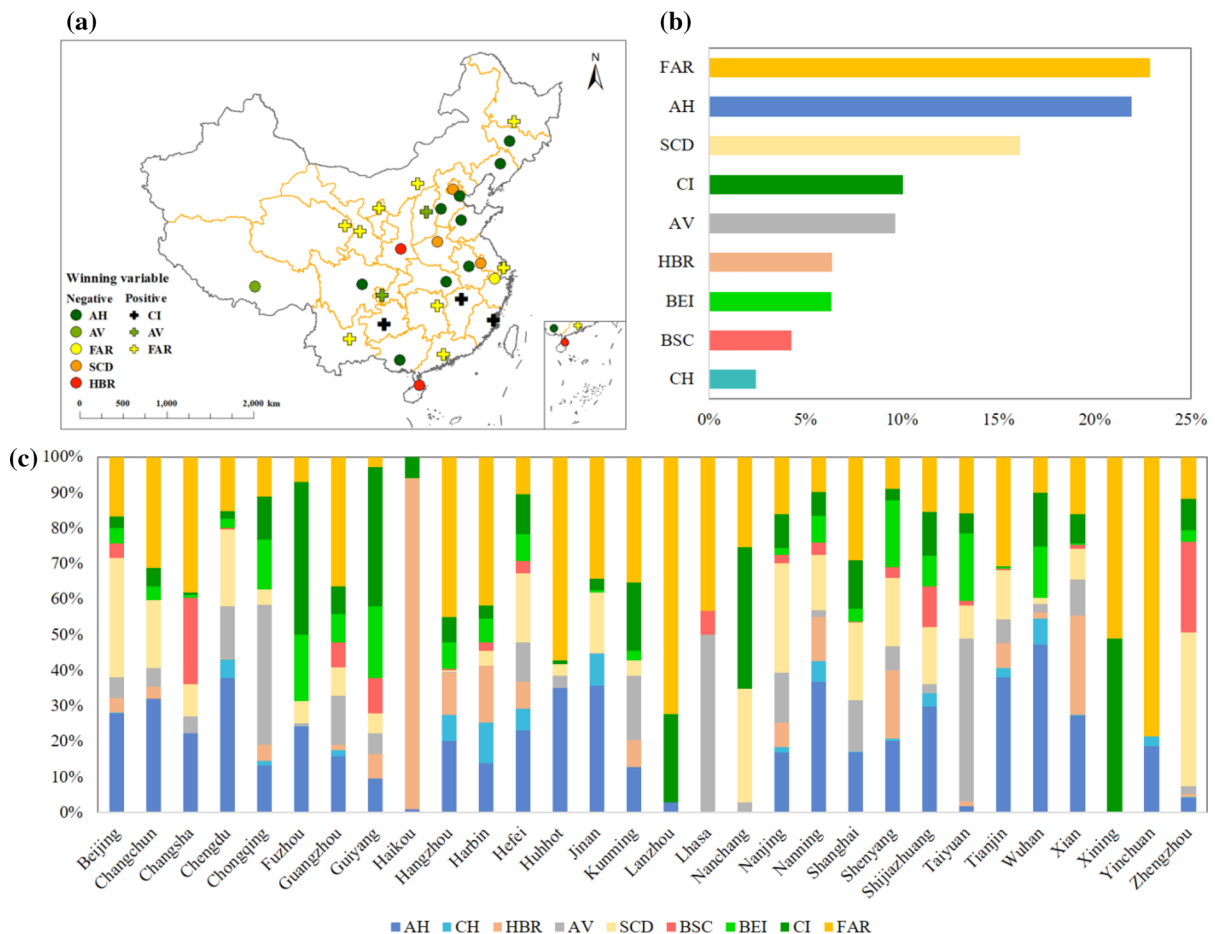


**Fig. 7** Summary statistics for winning variable of the GWR model. **a** spatial distribution of the dominant variable in 30 cities, **b** statistics of the winning variable in the whole grids, **c** statistics of the winning variable within each city grids

distribution of dominant variable for 30 cities. For the northern cities, the winning variables are mainly AH, while in northwestern cities, a notable impact of FAR is witnessed. In the southern cities, the situation is complicated, and AH, FAR and CI together exhibit a stronger influence.

Figure 7b and c show the statistics of the winning variables at the grid-cell scale. In the whole grids, note that FAR (22.88%) and AH (21.91%) are major winning variables, followed by SCD (16.12%) (Fig. 7b), while the remaining 6 factors show weaker influence. It is noted from Fig. 7c that due to larger area and stronger spatial heterogeneity of large cities, the winning variables vary with geographical location, meaning a variety of winning variables. However, for small cities, the type of winning variable is relatively unitary. Specifically, there are only three types of

winning variables in Haikou, Lanzhou, Lhasa and Yinchuan, and two types in Xining. In most cities, although the winning variable with the largest proportion is considered to be the main influencing factor of the city, the influence of the second or even third winning variable cannot be ignored.

The pseudo t-test was introduced to check the statistical significance of the regression coefficients for the explanatory variables. In general, the absolute value of T-statistic  $> 1.96$  indicates that the result is statistically significant at the 0.05 level (i.e., significance level P-value  $< 0.05$ ). The statistics of the directions for relationships between 3D landscape metrics and UHI in China's 30 cities are illustrated in Fig. 8. Overall, AH, HBR and SCD are negatively correlated with UHI, showing that high-rise buildings can help alleviate the UHI. AV, FAR and CI have a

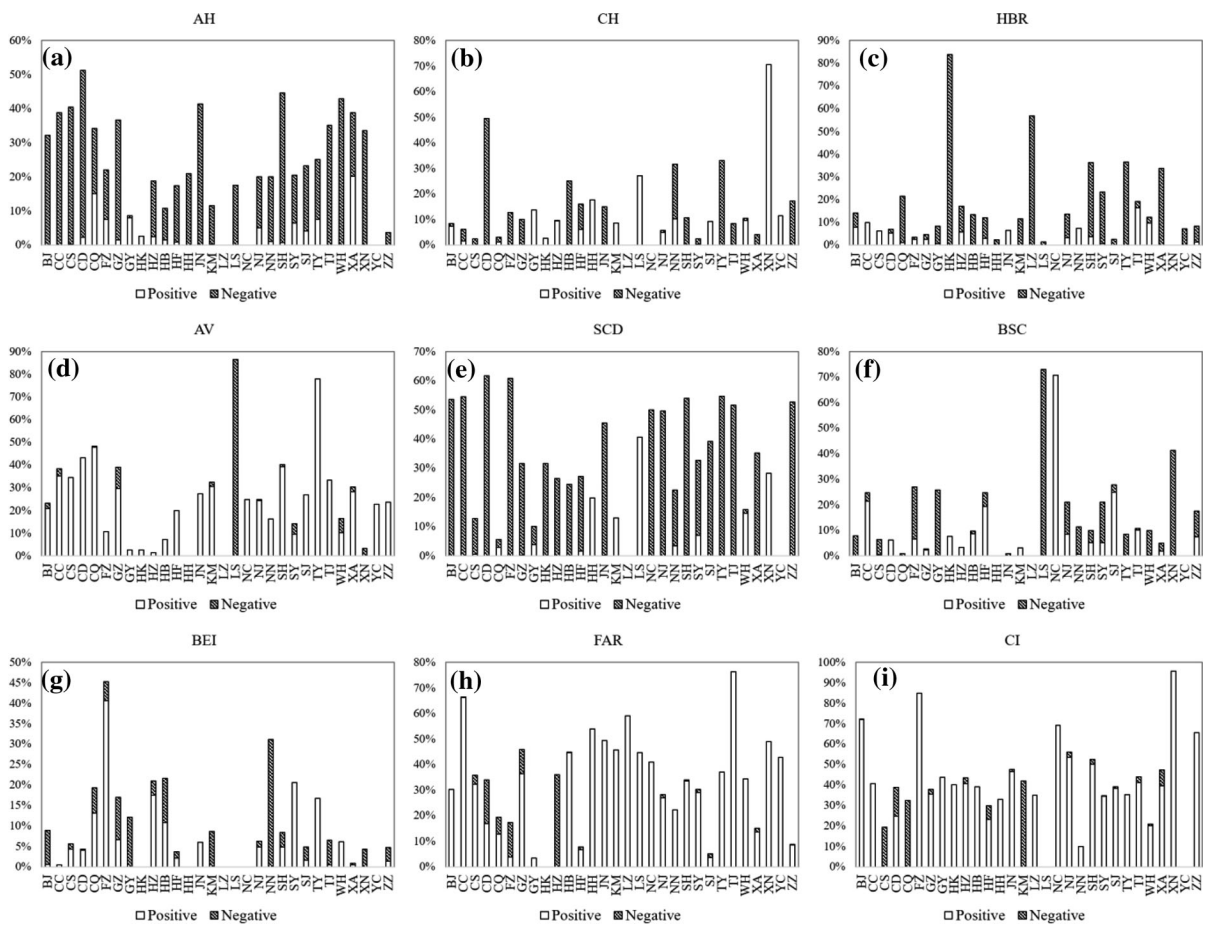


**Fig. 8** Statistics of the directions of relationships between 3D landscape metrics and UHI derived from the GWR model

positive correlation with UHI, indicating that the larger the buildings, the more crowded the buildings, and the more intense the UHI. But some exceptions cannot be avoided. More than 50% of the positive correlation between AH and UHI occurs in Xi'an and Chongqing. It is worth noting that in plateau cities of Lhasa and Xining, the AV shows a strong negative correlation with UHI. The negative correlation between FAR and UHI mainly occurred in Hangzhou, Guangzhou and Chongqing, accounting for more than 70%. For CH, BSC and BEI, which have less influence on the UHI, the direction of their correlations with UHI varies significantly between cities.

Statistical descriptions at the city scale blur some key details. From Fig. 8, for the three most important variables (FAR, AH and SCD) affecting UHI, something goes against the general rules, that is UHI is positively correlated with AH and SCD, and

negatively correlated with FAR in some study area, and the analysis on the grid-cell scale can explain this phenomenon. For AH, by calculating the building coverage ratio (BCR) of the positively correlated grids, it is found that the value is much lower than that of the negatively correlated grids (Fig. 9a, b). Since there are few buildings, the cooling effect of building height is difficult to play, and UHI may be dominated by other factors, such as vegetation. SCD works in similar way with AH. For FAR (Fig. 9c, d), the FAR value in the grids with negative FAR coefficient is generally lower than that in the grids with positive FAR coefficient, indicating that when the FAR of buildings is relatively low, higher FAR is related to lower LST.

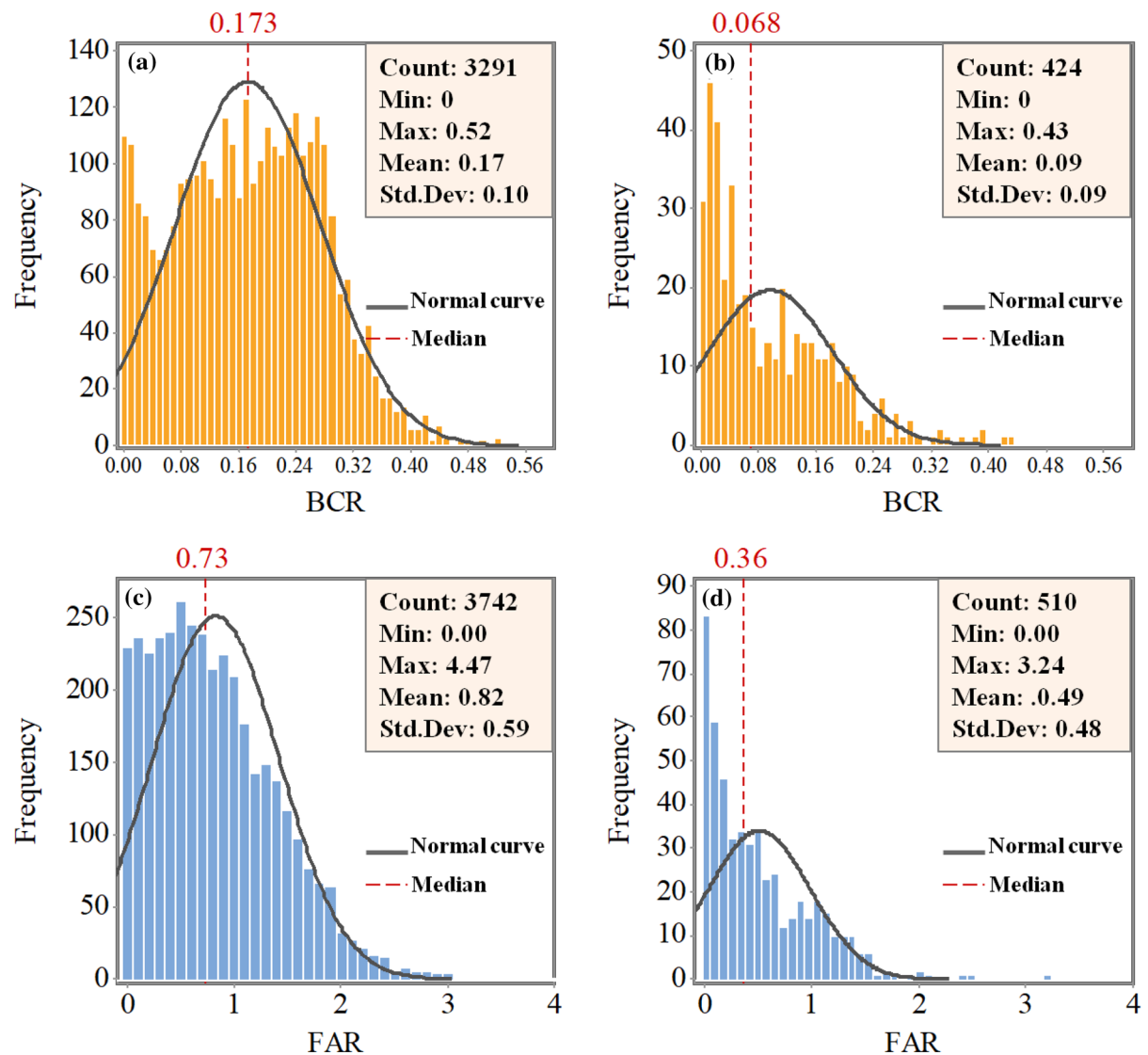


**Fig. 9** **a, b** Statistics of BCR in grids where AH coefficients are statistically significant. **a** Statistics of BCR in negative AH coefficient grids; **b** statistics of BCR in positive AH coefficient grids. **c, d** Statistics of FAR in grids where FAR coefficients are

statistically significant. **c** Statistics of FAR in positive FAR coefficient grids; **d** statistics of FAR in negative FAR coefficient grids

## Discussion

The general mechanism of 3D landscape metrics influencing UHI

Figure 7 shows that FAR outperforms the other 3D landscape metrics in influencing the UHI. Similar to previous study (Lan and Zhan 2017; Yin et al. 2018), for most cities, FAR significantly strengthens the UHI (Fig. 8h). FAR is a comprehensive urban planning

indicator to control the development intensity, which combined the building density and building height (Lan and Zhan 2017). For building density, high building density means that the impervious surface area with low albedo increases, thereby absorbing more solar radiation (Jamei and Rajagopalan 2017; Huang and Wang 2019). Besides, in areas with high building density, the ventilation conditions are not performing well, causing significant trapping of heat (Lin et al. 2017), and exacerbating the UHI.

Apparently, in grids with lower FAR, there is a negative correlation between FAR and UHI, especially in Hangzhou (Figs. 8h, 9c, d.). On the one hand, high density of buildings plays a critical role in reducing the amount of incoming solar radiation (Alavipanah et al. 2018). On the other hand, similar results were found in Bangkok (Pakarnseree et al. 2018), where higher FAR indicates higher buildings and larger shadows can lower the temperature. Our results further reveal the significant effect of FAR on UHI, i.e., it is not that the lower FAR is more favorable to the urban thermal environment. Reasonable building density is an effective means to alleviate the UHI.

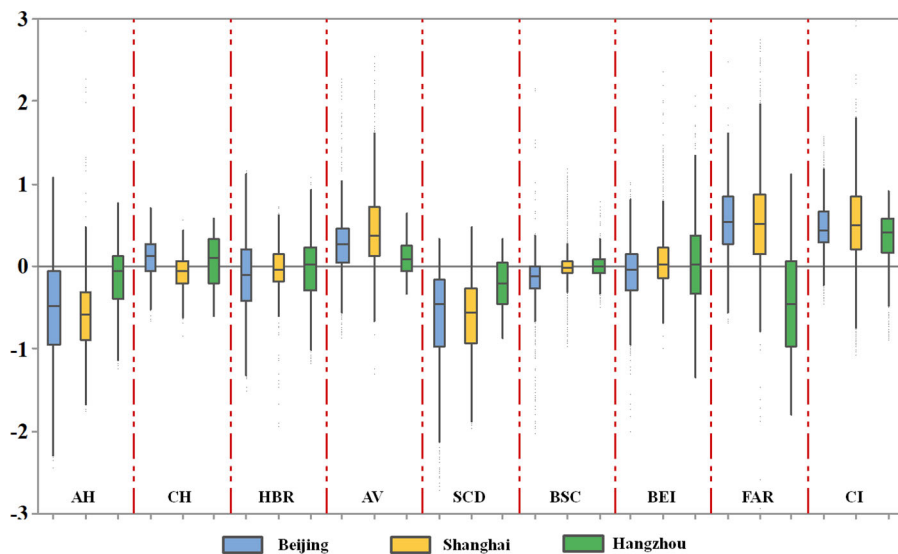
The impact of AH and SCD on UHI ranks second and third, respectively (Fig. 7a, b). SCD measures the congestion degree of buildings in 3D space, and it is closely related to the building height. Therefore, the impacts of SCD and AH are both negatively correlated with UHI. Other studies also reported the similar results in Beijing (Zheng et al. 2019), Shanghai (Sun et al. 2020), and Wuhan (Huang and Wang 2019). On the one hand, the higher the buildings, the larger the shadow they generate, which can decrease the solar radiation (Zheng et al. 2019). On the other hand, tall buildings can generate mechanical turbulence by improving surface roughness to enhance heat dissipation (Li et al. 2011). The positive correlation between AH and UHI mainly occurs in grids with low building coverage ratio (Fig. 9a, b). Alavipanah et al. (2018) confirmed that solar radiation will increase the surface temperature in areas without obstacles (buildings or vegetation cover). Yu et al. (2020) also found in Shanghai that the shadow effect does not work when the building shadows are not on low-albedo surfaces.

Figure 8 displays that both CI and AV are positively correlated with UHI. It results from that larger buildings can accommodate more human activities which would generate more heat (Yu et al. 2020). Moreover, larger buildings have larger surface areas, which increase the heat dissipation and the surrounding temperature (Huang and Wang 2019). While in plateau cities like Lhasa and Xining, the negative correlation between UHI and AV is caused by the thick walls of the buildings, which have good thermal insulation effects to prevent the loss of indoor heat (Wang et al. 2020). The negative impact of CH on the UHI is greater than the positive impact. One possible explanation is that a low CH value indicates that the height of the building is more uniform, thus

concentrating heat inside the compact structure and obstructing ventilation (Allegrini 2018). The positive correlation between BEI and UHI is mainly located in the periphery of the urban area, where gathering irregularly distributed factories and shanty towns. The inconsistent directions of the buildings block the air convection, so that the heat cannot be dissipated.

#### Typical case analysis of the impact of 3D landscape metrics on the UHI

The influence of 3D landscape metrics of buildings on the UHI has a general rule. However, it should be noted that the value of the GWR coefficient will be affected by the selection of city, because different cities have different architectural characteristics, landscapes, vegetation, and climate backgrounds (i.e., UHI have different driving mechanisms in different cities) (Li et al. 2020a, b). Three typical cities (Shanghai, Beijing and Hangzhou) were selected to analyze in detail the differences in the effects of different urban 3D landscape metrics on UHI. The results (Fig. 10) in Beijing and Shanghai are similar and consistent with the general mechanism, but there are still subtle differences. Shanghai's cooling effect of building height (AH, SCD) and warming effect of building volume (AV, CI) are significantly stronger than Beijing because of the higher and larger buildings in Shanghai (Figs. 2, 3, 10). Shanghai's FAR is much higher than Beijing (Figs. 2, 3), but compared with Beijing (Fig. 10), Shanghai's FAR warming effect is not prominent, which may be the offsetting effect of AH. But in Hangzhou, the effect of 3D landscape metrics (especially AH, SCD and FAR) on UHI is quite different from that of Beijing and Shanghai. Among the three cities, Hangzhou has the highest average building height (Figs. 2, 3), but Hangzhou's AH has the weakest alleviating effect on UHI (Fig. 10). One possible reason is that the mitigation impact of building height on UHI has a marginal effect, that is, when the building height is within 30 m, higher buildings are associated with lower LST. Otherwise, as the building height increases, the mitigation effect of building height on UHI will be weakened (Sun et al. 2020; Yu et al. 2020). Hangzhou has the lowest FAR among the three cities (Figs. 2, 3), and there is a strong negative correlation between Hangzhou's FAR and UHI, which indicates that the density of constructed buildings in Hangzhou is



**Fig. 10** The statistics of GWR coefficients in Beijing, Shanghai, and Hangzhou

moderate to avoid the penetration of hot solar radiation, thus reducing the LST. Urban planning should not blindly emphasize the reduction of building density. A reasonable planning of building density can alleviate UHI, just like Hangzhou.

#### Effects of UHI

Previous studies have shown that urban building patterns can cause the UHI by affecting the distribution of energy balance (Yue et al. 2019). Due to the contradiction between the rapid growth of urban population and the shortage of construction land, the city is expanding rapidly in the two-dimensional direction, as well as the extension of urban buildings height (Chun and Guldmann 2014), which has greatly changed the characteristics of the atmosphere and the surface properties, thereby changing the city's energy balance and affecting the city's thermal environment (Yue et al. 2019; Hu et al. 2020). UHI has been documented in more than 400 major cities around the world (Haddad et al. 2020), which is the most typical characteristics of world urban climate. Currently, more than half of the world's population lives in urban areas, and by 2030, this number is expected to reach 67% (Seto et al. 2012; Chapman et al. 2017). It means that more people will face more frequent and intensified extreme heat events in the future, no mention that demographic changes and an increase in

the proportion of vulnerable elderly people (Li et al. 2020b). As the severity of the UHI increases, problems related to human life and the ecological environment may become more serious (Zhou et al. 2014b). How to alleviate the UHI effect scientifically, effectively and practically has become one of the key issues of concern worldwide (Ma et al. 2016; Lin et al. 2017). By affecting the surface energy balance process and air flow, the 3D landscape pattern of the buildings changes the thermal environment, and greatly intensify the UHI, which has been confirmed worldwide (Berger et al. 2017; Pakarnseree et al. 2018; Huang and Wang 2019; Hu et al. 2020; Sun et al. 2020). Some studies even prove that the impact of 3D landscape metrics on UHI is more important than 2D landscape metrics (Alavipanah et al. 2018; Tian et al. 2019; Yu et al. 2020). It is extremely necessary to reduce the UHI and achieve sustainable development through rationally planning the buildings in 3D space. In 2015, the Political Bureau of the Central Committee put forward a new concept of “greenization”, which refers to an environment-friendly and resource-saving development pattern (Zhang et al. 2019a). Therefore, it is necessary to scientifically plan the 3D pattern of urban buildings to ensure the balance between urban thermal environment and socioeconomic development, and economic development should be carried out in a more sustainable and friendly way (Wu 2014).

## Implications and limitations

The measure of optimizing the 3D building landscape metrics through urban planning to achieve the mitigation of UHI is not only feasible, but also effective, since that the relative importance of 3D landscape metrics has been proven to be greater than 2D landscape metrics (Alavipanah et al. 2018; Yu et al. 2020). The relationship between the 3D landscape metrics and UHI revealed by this research can help to minimize the impact of urbanization on UHI through targeted building planning, which is of great significance to urban ecological security and sustainable development, and can provide important scientific basis for urban ecological planning and landscape design.

From the perspective of the spatial distribution characteristics of the impact of the 3D landscape metrics on the UHI, for northern cities, the UHI can be significantly alleviated by reducing the floor space of buildings to reduce the FAR while increasing the height of the buildings; for southern cities, in addition to the above two points, it is necessary to appropriately reduce the volume of the buildings. Specific to the impact of each important 3D landscape metric, (1) for FAR, AH and SCD, when constructing a building, moderate vertical expansion can be used to replace the horizontal expansion of the building, which can not only ensure the temperature reduction function of high-rise buildings, but also reduce the building floor area, achieving the purpose of decreasing the building density. Meanwhile, instead of blindly reducing the FAR of buildings, policy makers can take the FAR value in Hangzhou buildings as the standard for planning. However, the planners should specially pay attention to the two cities pointed out in “[The general mechanism of 3D landscape metrics influencing UHI](#)” section—Chongqing and Xi'an. On the outskirts of these two cities, the UHI is exacerbated due to the mismatch of building height and coverage, so it is better to appropriately reduce the height of the buildings and increase the number of buildings; (2) for AV and CI, it is necessary to reduce the volume of buildings as much as possible, but for plateau cities like Lhasa and Xining, the increase of building volume will greatly help to alleviate the UHI; (3) for CH, construct new buildings of different heights to ensure that the canyon wind generated by the staggered buildings is easy to dissipate heat except for cities in

northwest and southwest; (4) for BEI, some irregular factories and shantytowns outside the urban area can be re-planned and constructed to ensure that the buildings share a unified direction, thereby enhancing air convection and dissipating heat.

There are still several limitations in this study. Firstly, the impact of 3D landscape metrics on UHI was only analyzed in summer, while other seasons were not considered. In fact, the impact of the 3D landscape metrics on the UHI varies with the seasons (Hu et al. 2020). Secondly, since Landsat data were only available at daytime, nighttime UHI was not considered in this study. Studies have shown that the thermal mass of buildings, heated during the day, slowly releases the heat at night, causing the LST to rise. This process might be related to the density, height and materials of buildings (Monteiro et al. 2021). However, due to data limitations, the effect of 3D building spatial pattern on nighttime UHI has not been fully explored to reach a conclusion. In future study, both daytime and nighttime LST data (e.g., low-resolution MODIS data) may be introduced to explore the relationships between 3D landscape metrics and UHI. Lastly, the relationship between 3D landscape metrics and UHI was analyzed only in the urban core area due to the lack of building data in the urban fringe. In future, we will continue to collect complete building data to explore the differences between urban and suburban areas, which will be of great significance for improving the urban thermal environment.

## Conclusion

This study investigates the effects of 3D building landscape pattern on summer UHI among 30 megacities of China by GWR model at both micro grid-cell scale and macro city scale. The conclusion shows that China's 30 provincial capitals/municipalities are experiencing varying degrees of UHI, and the GWR model accurately confirms that the 3D landscape pattern of buildings greatly affects the urban heat islands. Especially, at the city scale, FAR and AH become the most important 3D landscape metrics affecting the UHI, and the analysis at the grid-cell scale also proves that SCD is the third most important variable, while HBR, BEI, BSC, and CH are less important. Generally speaking, at city scale, AH and SCD are negatively correlated with UHI, while FAR is

positively correlated with the UHI. The increase in AV and CI will also exacerbate the heat island effect. It is worth noting that the relationships between 3D landscape pattern and UHI exhibited obvious spatial heterogeneity. For different cities and grids, the magnitude and even the direction (positive and negative) of the impact of the same 3D landscape metric will change. Unable to block hot solar radiation, the UHI was found to be more intense in areas with low FAR. In areas with low BCR, the cooling effect of AH of buildings is difficult to achieve. In plateau cities, due to the characteristics of buildings formed under the alpine climate, AV and UHI are negatively correlated. Therefore, it is necessary to fully consider the actual situation when making urban architectural plans. The relationship between the 3D landscape pattern of buildings and the UHI revealed by this study provides a reference for how to improve the thermal conditions and further promote urban ecological security through reasonable architectural planning and management.

**Author contributions** All authors of this research paper have directly participated in the planning, execution, or analysis of the study.

**Acknowledgements** We sincerely appreciate editor Jingle Wu and three anonymous reviewers for their comments on previous versions of the manuscript, which invited us to reconsider some of our ideas and clearly helped to improve the manuscript. This research was supported by the National Natural Science Foundation Projects of China (Nos. 41701484 and 41601459), Hubei Chengguang Talented Youth Development Foundation, Chengguang Program of Shanghai Education Development Foundation and Shanghai Municipal Education Commission (No. 17CG45).

**Data availability** The datasets generated during and analyzed during the current study are not publicly available due to confidentiality but are available from the corresponding author on reasonable request.

**Code availability** Not applicable.

## Declarations

**Conflict of interest** The authors have no relevant financial or non-financial interests to disclose.

**Ethical approval** The contents of this manuscript have not been copyrighted or published previously. The contents of this manuscript are not under consideration for publication

elsewhere. There are no directly related manuscripts or abstracts, published or unpublished, by any author(s) of this paper.

**Consent to participate** All authors of this paper are consent to participate.

**Consent for publication** All authors of this paper are consent for publication.

## References

- Akaike H (1998) Information theory and an extension of the maximum likelihood principle. Selected Papers of Hirotugu Akaike. Springer Series in Statistics (Perspectives in Statistics). Springer, New York, NY. [https://doi.org/10.1007/978-1-4612-1694-0\\_15](https://doi.org/10.1007/978-1-4612-1694-0_15)
- Alavipanah S, Schreyer J, Haase D, Lakes T, Qureshi S (2018) The effect of multi-dimensional indicators on urban thermal conditions. *J Clean Prod* 177:115–123
- Allegrini J (2018) A wind tunnel study on three-dimensional buoyant flows in street canyons with different roof shapes and building lengths. *Build Environ* 143:71–88
- Berger C, Rosentreter J, Voltersen M, Baumgart C, Schmullius C, Hese S (2017) Spatio-temporal analysis of the relationship between 2D/3D urban site characteristics and land surface temperature. *Remote Sens Environ* 193:225–243
- Brunsdon C, Fotheringham A, Charlton ME (1996) Geographically weighted regression: a method for exploring spatial nonstationarity. *Geogr Anal* 28:281–298
- Cao Q, Liu Y, Georgescu M et al (2020) Impacts of landscape changes on local and regional climate: a systematic review. *Landsc Ecol* 35:1269–1290
- Chapman S, Watson JEM, Salazar A et al (2017) The impact of urbanization and climate change on urban temperatures: a systematic review. *Landsc Ecol* 32:1921–1935
- Chun B, Guldmann JM (2014) Spatial statistical analysis and simulation of the urban heat island in high-density central cities. *Landsc Urban Plan* 125(3):76–88
- Connors JP, Galletti CS, Chow WTL (2013) Landscape configuration and urban heat island effects: assessing the relationship between landscape characteristics and land surface temperature in Phoenix, Arizona. *Landsc Ecol* 28:271–283
- Defries RS, Townshend JRG (2007) Townshend NDVI-derived land cover classifications at a global scale. *Int J Remote Sens* 15:3567–3586
- Fang C, Wang S, Li G (2015) Changing urban forms and carbon dioxide emissions in China: a case study of 30 provincial capital cities. *Appl Energy* 158:519–531
- Feyisa GL, Meilby H, Jenerette GD, Pauliet S (2016) Locally optimized separability enhancement indices for urban land cover mapping: exploring thermal environmental consequences of rapid urbanization in Addis Ababa, Ethiopia. *Remote Sens Environ* 175:14–31
- Fotheringham AS, Brunsdon C, Charlton M (2004) Geographically weighted regression: the analysis of spatially varying relationships. *Am J Agr Econ* 86 (2):554–556. [https://doi.org/10.1111/j.0002-9092.2004.600\\_2.x](https://doi.org/10.1111/j.0002-9092.2004.600_2.x)

- Getis A, Ord JK (1992) The analysis of spatial association by use of distance statistics. *Geogr Anal* 24:189–206
- Haddad S, Paolini R, Ulpiani G, Synnefa A, Hatvani-Kovacs G, Garshasbi S, Fox J, Vasilakopoulou K, Nield L, Santamouris M (2020) Holistic approach to assess co-benefits of local climate mitigation in a hot humid region of Australia. *Sci Rep* 10:14216
- Hu Y, Dai Z, Guldmann JM (2020) Modeling the impact of 2D/3D urban indicators on the urban heat island over different seasons: a boosted regression tree approach. *J Environ Manag*. <https://doi.org/10.1016/j.jenvman.2020.110424>
- Huang G, Cadenasso ML (2016) People, landscape, and urban heat island: dynamics among neighborhood social conditions, land cover and surface temperatures. *Landscape Ecol* 31:2507–2515
- Huang X, Wang Y (2019) Investigating the effects of 3D urban morphology on the surface urban heat island effect in urban functional zones by using high-resolution remote sensing data: a case study of Wuhan, Central China. *ISPRS J Photogram Remote Sens* 152:119–131
- Jamei E, Rajagopalan P (2017) Urban development and pedestrian thermal comfort in Melbourne. *Sol Energy* 144:681–698
- Jia SQ, Wang YH (2020) Effects of land use and land cover pattern on urban temperature variations: a case study in Hong Kong. *Urban Clim*. <https://doi.org/10.1016/j.uclim.2020.100693>
- Jun-Hyun K, Gu D, Wonmin S, Sung-Ho K, Hwanyong K, Dong-Kun L (2016) Neighborhood landscape spatial patterns and land surface temperature: an empirical study on single-family residential areas in Austin, Texas. *Int J Environ Res Public Health* 13(9):880
- Kong LQ, Liu ZF, Wu JG (2020) A systematic review of big data-based urban sustainability research: state-of-the-science and future directions. *J Clean Prod*. <https://doi.org/10.1016/j.jclepro.2020.123142>
- Lan Y, Zhan Q (2017) How do urban buildings impact summer air temperature? The effects of building configurations in space and time. *Build Environ* 125:88–98
- Li SC, Zhao ZQ, Miaoqiao X, Wang YL (2010) Investigating spatial non-stationary and scale-dependent relationships between urban surface temperature and environmental factors using geographically weighted regression. *Environ Model Softw* 25(12):1789–1800
- Li J, Song C, Cao L, Zhu F, Meng X, Wu J (2011) Impacts of landscape structure on surface urban heat islands: a case study of Shanghai, China. *Remote Sens Environ* 115:3249–3263
- Li L, Zha Y, Zhang JH (2020a) Spatially non-stationary effect of underlying driving factors on surface urban heat islands in global major cities. *Int J Appl Earth Obs Geoinf*. <https://doi.org/10.1016/j.jag.2020.102131>
- Li Y, Schubert S, Kropp JP et al (2020b) On the influence of density and morphology on the Urban Heat Island intensity. *Nat Commun* 11:2647
- Lin P, Siu S, Qin H, Gou Z (2017) Effects of urban planning indicators on urban heat island: a case study of pocket parks in high-rise high-density environment. *Landscape Ecol* 32(7):48–60
- Liu M, Hu YM, Li CL (2017) Landscape metrics for three-dimensional urban building pattern recognition. *Appl Geogr* 87:66–72
- Liu Y, Chen C, Li J et al (2020a) Characterizing three dimensional (3-D) morphology of residential buildings by landscape metrics. *Landscape Ecol* 35:2587–2599
- Liu Y, Fei X, Zhang Z, Li Y, Tang J, Xiao R (2020b) Identifying the sources and spatial patterns of potentially toxic trace elements (PTEs) in Shanghai suburb soils using global and local regression models. *Environ Pollut*. <https://doi.org/10.1016/j.envpol.2020.114171>
- Ma Q, Wu J, He C (2016) A hierarchical analysis of the relationship between urban impervious surfaces and land surface temperatures: spatial scale dependence, temporal variations, and bioclimatic modulation. *Landscape Ecol* 31:1139–1153
- Monteiro FF, Gonçalves WA, Andrade L, Villavicencio L, Silva C (2021) Assessment of Urban Heat Islands in Brazil based on MODIS remote sensing data. *Urban Clim*. <https://doi.org/10.1016/j.uclim.2020.100726>
- Morabito M, Crisci A, Messeri A, Orlandini S, Raschi A, Maracchi G, Munafò M (2016) The impact of built-up surfaces on land surface temperatures in Italian urban areas. *Sci Total Environ* 551–552:317–326. <https://doi.org/10.1016/j.scitotenv.2016.02.029>
- NASA (2019) Landsat 8 data users Handbook. <http://landsathandbook.gsfc.nasa.gov/>
- Oke TR (1973) City size and the urban heat island. *Atmos Environ* 7(8):769–779
- Ord JK, Getis A (1995) Local spatial autocorrelation statistics: distributional issues and an application. *Geogr Anal* 27:286–306
- Pakarnseree R, Chunkao K, Bualert S (2018) Physical characteristics of Bangkok and its urban heat island phenomenon. *Build Environ* 143:561–569
- Peng J, Jia JL, Liu YX, Li HL, Wu JS (2018) Seasonal contrast of the dominant factors for spatial distribution of land surface temperature in urban areas. *Remote Sens Environ* 215:255–267
- Seto KC, Güneralp B, Hutyra LR (2012) Global forecasts of urban expansion to 2030 and direct impacts on biodiversity and carbon pools. *Proc Natl Acad Sci USA* 109:16083–16088
- Sun RH, Lü YH, Yang XJ, Chen LD (2019) Understanding the variability of urban heat islands from local background climate and urbanization. *J Clean Prod* 208:743–752
- Sun FY, Liu M, Wang YC, Wang H, Che Y (2020) The effects of 3D architectural patterns on the urban surface temperature at a neighborhood scale: relative contributions and marginal effects. *J Clean Prod*. <https://doi.org/10.1016/j.jclepro.2020.120706>
- Szymański M, Kryza M (2012) Local regression models for spatial interpolation of urban heat island—an example from Wrocław, SW Poland. *Theor Appl Climatol* 108:53–71
- Tian Y, Zhou W, Qian Y, Zheng Z, Yan JL (2019) The effect of urban 2D and 3D morphology on air temperature in residential neighborhoods. *Landscape Ecol* 34:1161–1178
- United Nations (2019) World population prospects 2019: highlights. <https://www.un.org/development/desa/>

- [publications/world-population-prospects-2019-highlights.html](https://www.un.org/weltbevölkerung/prospekte-2019-highlights.html)
- Wang J, Qian YG, Han LJ, Zhou WQ (2016) Relationship between land surface temperature and land cover types based on GWR model: a case study of Beijing-Tianjin-Tangshan urban agglomeration, China. *Chin J Appl Ecol* 27(7):2128–2136
- Wang XL, Mai XM, Lei B, Bi HQ, Zhao B, Mao G (2020) Collaborative optimization between passive design measures and active heating systems for building heating in Qinghai-Tibet plateau of China. *Renew Energy* 147:683–694
- Weng YC (2007) Spatiotemporal changes of landscape pattern in response to urbanization. *Landscape Urban Plan* 81:341–353
- Wu JG (2004) Effects of changing scale on landscape pattern analysis: scaling relations. *Landscape Ecol* 19(2):125–138
- Wu JG (2010) Urban sustainability: an inevitable goal of landscape research. *Landscape Ecol* 25:1–4
- Wu JG (2014) Urban ecology and sustainability: the state-of-the-science and future directions. *Landscape Urban Plan* 125:209–221
- Wu CD, Lung C (2016) Application of 3-D urbanization index to assess impact of urbanization on air temperature. *Sci Rep* 6:1–9
- Wu CD, Chun S, Lung C, Jan JF (2013) Development of a 3-D urbanization index using digital terrain models for surface urban heat island effects. *ISPRS J Photogram Remote Sens* 81:1–11
- Yang Q, Huang X, Tang Q (2019) The footprint of urban heat island effect in 302 Chinese cities: temporal trends and associated factors. *Sci Total Environ* 655:652–662
- Yin C, Yuan M, Lu Y, Huang YP, Liu YF (2018) Effects of urban form on the urban heat island effect based on spatial regression model. *Sci Total Environ* 634:696–704
- Yu SY, Chen ZQ, Yu BL, Wang L, Wu B, Wu JP, Zhao F (2020) Exploring the relationship between 2D/3D landscape pattern and land surface temperature based on explainable eXtreme Gradient Boosting tree: a case study of Shanghai, China. *Sci Total Environ*. <https://doi.org/10.1016/j.scitotenv.2020.138229>
- Yue WZ, Liu X, Zhou YY, Liu Y (2019) Impacts of urban configuration on urban heat island: an empirical study in China mega-cities. *Sci Total Environ* 671:1036–1046
- Zhang PF, Hu YM (2013) Variations of three-dimensional architecture landscape at different spatial scales. *Chin J Ecol* 32(5):1319–1325
- Zhang P, Yuan H, Tian X (2019a) Sustainable development in China: trends, patterns, and determinants of the “Five Modernizations” in Chinese cities. *J Clean Prod* 214:685–695
- Zhang Y, Middel A, Turner BL (2019b) Evaluating the effect of 3D urban form on neighborhood land surface temperature using Google Street View and geographically weighted regression. *Landscape Ecol* 34:681–697
- Zheng Z, Zhou WQ, Yan JL, Qian YG, Wang J, Li WF (2019) The higher, the cooler? Effects of building height on land surface temperatures in residential areas of Beijing. *Phys Chem Earth Parts A/B/C* 110:149–156
- Zhou DC, Zhao SQ, Liu SG, Zhang LX, Zhu C (2014a) Surface urban heat island in China’s 32 major cities: spatial patterns and drivers. *Remote Sens Environ* 152:51–61
- Zhou W, Qian Y, Li X et al (2014b) Relationships between land cover and the surface urban heat island: seasonal variability and effects of spatial and thematic resolution of land cover data on predicting land surface temperatures. *Landscape Ecol* 29:153–167

**Publisher's Note** Springer Nature remains neutral with regard to jurisdictional claims in published maps and institutional affiliations.